


Processing and Property Characterization of Zn Acceptor/Sn Donor Codoped Gallium Nitride Films Prepared by Reactive Sputtering with a Cermet Target

DONG-HAU KUO ^{1,3}, YEN-TZU LIU,¹ and DER-JUN JAN²

1.—Department of Materials Science and Engineering, National Taiwan University of Science and Technology, Taipei 10607, Taiwan. 2.—Physics Division, Institute of Nuclear Energy Research (INER), Longtan District, Taoyuan City 32546, Taiwan. 3.—e-mail: dhkuo@mail.ntust.edu.tw

Codoping zinc (Zn) and tin (Sn) in forming quaternary acceptor/donor codoped gallium nitride thin films using reactive sputtering technique under a cermet target is presented in this study. The purpose of codoping in GaN is to extend its electrical properties to a wider range through defect engineering. There are few reports on the Zn/Sn codoped GaN thin films by chemical or physical processes at this stage. To develop the acceptor/donor codoped GaN, this work was focused on the influence of process parameters of deposition temperatures and RF sputter power on the film properties in order to explore the defect behaviors. RF sputter power showed a strong effect on the performance of *p*-type Zn/Sn-GaN films, with the hole concentration in the range of 9.5×10^{12} – $5.1 \times 10^{17} \text{ cm}^{-3}$, electrical conductivity of 1.5×10^{-6} – 1.1 S cm^{-1} , and optical band gap of 2.92–3.22 eV. On the other hand, the effect of deposition temperature on properties was not noticeable.

Key words: GaN, codoping, Zn acceptor, Sn donor, sputtering, electrical property

INTRODUCTION

Gallium nitride (GaN) is an important III–V semiconductor for electronic and optoelectronic devices. GaN can form the tertiary and quaternary alloy systems with the combinations of AlN, GaN, and InN to achieve a wide range of bandgap values. The best-known report for GaN has been about Prof. S. Nakamura, as one of the three recipients for the 2014 Nobel Prize in Physics for his contribution in developing *p*-type, Mg-doped GaN.

GaN, as an intrinsic semiconductor, has attracted attention for its doping modifications. The popular *p*-type dopants are Zn and Mg and the *n*-types are Si, Ge, and Sn. Because of the emergent needs of *p*-type GaN for diodes and transistors, Zn- and Mg-doped GaN films have been commercially used in the epitaxial form. From the viewpoint of electronic

devices, pure GaN epitaxial film is used for *n*-GaN and the heavily doped n^+ GaN film is for the electrode contact. The incorporation of Si, Ge, and Sn into *n*-GaN films have few reports. Nakamura et al. showed that Ge-GaN prepared with a GeH_4 precursor and Si-GaN films with SiCl_4 showed the high electron concentrations above 10^{19} cm^{-3} .¹ Molina et al. fabricated a Si-GaN layer with a SiH_4 precursor by MBEs, and they confirmed that Si doping led to more planar defects.² As Sn-GaN was developed for *n*-type GaN with metalorganic chemical vapor deposition (MOCVD),³ our group demonstrates the electrical properties of Sn-GaN films fabricated by reactive sputtering with a cermet target.⁴

There are also few data reported for the acceptor/donor codoped GaN films, as the deposition system is much more complex and expansive for MOCVD. Si and Zn codoped InGaN has been used for the broad band emission of InGaN/AlGaN LEDs, which showed high efficiency through the donor–acceptor (DA) pair recombination.^{5,6} *n*-type GaN

with Si and Zn co-doping has shown exceptionally high absolute internal quantum efficiency above 90% for the blue luminescence.⁷ Mg/Si codoped *p*-type GaN was studied for obtaining the high conductivity.⁸ The effect of Eu-Mg defects associated with the DA pair in GaN on the temperature-dependence photoluminescence was evaluated.⁹ However, the multiple-component III nitride films are difficult for the MOCVD system to execute. Therefore, the works on DA pairs have been few. Recently, codoping effects of Ge donor/Zn acceptor and Sn donor/Zn acceptor for GaN thin films on properties and device performance have been issued from our group with a simple sputtering system.^{10,11} Our data have shown that the codoping method enhanced the solubility of the dopant, reduced the acceptor energy level, and increased the mobility of the carriers.¹²

In addition to the application for electronic devices, GaN-based semiconductors have also attracted attention as a photoelectrode for their potential in water splitting.^{13,14} After mixing with ZnO, a solid solution of GaN and ZnO or (Ga,Zn)(O,N) and its modified composite with Rh-Cr₂O₃ show exceptional hydrogen production rates.^{15,16} (Ga,Zn)(O,N) can be viewed as a degenerate GaN semiconductor heavily incorporated with a Zn acceptor and O donor. The MOCVD process for GaN at high temperatures above 800°C is not suitable for sensing and photocatalysis. For the sake of extending GaN application, a low-temperature process for GaN and its degenerate derivatives is welcomed. Our group has developed a low-temperature reactive sputtering technique with single cermet targets for GaN, InGaN, AlInGaN, and their counterparts with Sn, Zn, Mg, and Ge doping.^{4,17–23} Basically, different modifications for GaN films can be achieved with this sputtering technique. The electron conductivity of the *n*-type GaN was enhanced with the Sn and Ge donors, but their mobility was greatly decreased.^{4,22} However, a Sn dopant greatly lowered the optical band gap (E_g), while Ge did not have an effect on E_g . For the acceptor doping with Zn and Mg, *p*-type GaN formed through *n*-type GaN with the doping concentration.^{18,21} Mg-GaN showed the greater mobility of 345 cm² V⁻¹ s⁻¹ and conductivity of 3.23 S cm⁻¹. 5%Al doping in InGaN showed an extremely high mobility of 1200 cm² V⁻¹ s⁻¹, but had greatly lowered the high electron concentration of 10¹⁹ cm⁻³ for In_{0.2}Ga_{0.8}N to 6.75 × 10¹⁷ cm⁻³ for AlInGaN.²³ Based upon our work, the optical band gap, electrical properties, the type of carrier, etc. for a wide range of compositions in the sputtered GaN can be predicted. The database for the materials design of sputtered GaN films can be established.

Different from our previous work for films deposited at different target compositions to understand the performance in variation with the Zn content in targets, here Zn/Sn-codoped GaN thin films on Si (100) wafers were deposited at different

growth temperatures and RF sputter powers. Because of the importance of the GaN-based materials, it is our purpose to establish the database of the materials properties for III-nitride semiconductors at different sputtering conditions in order for materials selection and design with a cost-effective, safe, and environment-friendly approach. These GaN-based properties data, such as electrical and optical properties, also provide insight for photocatalysis, electrolysis, and electrochemistry.

EXPERIMENTAL PROCEDURES

Zn acceptor/Sn donor codoped GaN or Zn/Sn-GaN thin films were prepared on Si (100) substrates by the technique of radio-frequency (RF) reactive sputtering with a cermet target at different deposition temperatures of 100–400°C while keeping sputtering power at 120 W or at different sputter powers of 90–150 W while keeping the growth temperature at 400°C. The cermet target was made by hot pressing with a mold filled with Ga, Zn, Sn, and GaN powders for the design composition of (Ga_{0.9}Zn_{0.06}Sn_{0.04})N. Before loading the pressure, the hot press furnace was mechanically pumped down to avoid the target oxidation. For reactive sputtering deposition, the chamber needs to use the diffusion pump for a low pressure of 1.33 × 10⁻⁷ kPa, before sputtering at 1.2 × 10⁻³ kPa. The Ar flow rate of 5 sccm was used for plasma generation and the N₂ flow rate of 10 sccm was used for the nitridation reaction.

X-ray diffractometry (XRD, D8 Discover, Bruker) and high-resolution transmission electron microscopy (HR-TEM, Technai G2, Philips) were used for analyzing the crystal structure of Zn/Sn-GaN films. Scanning electron microscopy (SEM, JSM-6500F, JEOL) and atomic force microscopy (AFM, Dimension Icon, Bruker) were used to evaluate the surface morphology and topography. Energy dispersive spectrometer (EDS, JSM-6500F, JEOL) equipped on SEM was for compositional analyses. Electrical properties were measured with a Hall measurement system (HMS-2000, Ecopia). The absorption spectra were measured with an ultraviolet-visible (UV-Vis) spectrometer (V-670, Jasco).

RESULTS AND DISCUSSION

Compositions of the Zn/Sn-GaN films prepared at different temperatures of 100–400°C and different RF sputter powers of 90–150 W were obtained with EDS, as shown in Table I. For films processed at different temperatures, their film compositions stayed similar. Under 120 W, the deposition temperature is not a process parameter to change the film composition. All the films were viewed to have an average [Zn]/([Zn] + [Sn] + [Ga]) ratio of 0.063 and average [Sn]/([Zn] + [Sn] + [Ga]) ratio of 0.048, which were close to the design composition of (Ga_{0.9}Zn_{0.06}Sn_{0.04})N. The N content for different samples showed an average [N]/([Zn] + [Sn] + [Ga]) ratio of 0.910, indicating that all these films were

Table I. Compositional analyses of Zn acceptor/Sn donor-codoped GaN films prepared at different deposition temperatures of 100–400°C, while keeping RF sputter power of 120 W, and at different sputter powers of 90–150 W, while keeping at 400°C

Sputter power (W)	Deposition temp. (°C)	Ga (at.%)	Zn (at.%)	Sn (at.%)	N (at.%)	[Zn]/[Ga + Sn + Zn]	[Sn]/[Ga + Sn + Zn]	[N]/[Ga + Sn + Zn]
120	100	47.4	3.32	2.66	46.62	0.062	0.049	0.873
120	200	46.13	3.19	2.68	48.0	0.061	0.051	0.923
120	300	45.13	3.71	2.63	48.53	0.062	0.045	0.943
120	400	46.69	3.47	2.48	47.36	0.066	0.047	0.900
90	400	53.62	3.14	2.44	40.8	0.053	0.041	0.689
150	400	47.21	3.37	1.59	47.83	0.065	0.031	0.917

slightly deficient in nitrogen. The Zn/Sn-GaN films contained a donor defect in nitrogen vacancy. For films processed at different RF sputter powers, there was a major difference in the N ratio. The 90 W-deposited Zn/Sn-GaN film was strongly deficient in N content with a $[N]/([Zn] + [Sn] + [Ga])$ ratio of 0.689. The N strong deficiency in N for the Zn/Sn-GaN films can have three possible conditions: form a nitrogen deficiency, metal interstitials, or precipitates at grain boundaries from incorporation of Zn and Sn. A minor difference was a slightly lower Sn content in the 150 W-deposited film with a $[Sn]/([Zn] + [Sn] + [Ga])$ ratio of 0.31. The possible reason for the lower Sn content in film made at 150 W is related to the high power in reactive sputtering to facilitate the easier vaporization of the already deposited Sn in films.

Figure 1 shows XRD spectra of the Zn/Sn-GaN films grown at different substrate temperatures and at different RF sputter powers. For the effect of deposition temperature, as shown in Fig. 1a–d, XRD data indicated that all Zn/Sn-GaN films were in the polycrystalline form and formed a Wurtzite structure, which showed a preferential (10 $\bar{1}$ 0) growth plane with a diffraction peak located at $2\theta = 32.15^\circ$. Other diffraction peaks were weak and related to the (0002), (10 $\bar{1}$ 1), and (11 $\bar{2}$ 0) growth planes. No second phases were detected. The peak positions were close for films deposited at 100–400°C, because they had close composition (Table I). Lattice constants of a and c , and the volume of unit cell for Zn/Sn-GaN films grown at different conditions, were close and the average dimensions were 3.21 Å, 5.2 Å, and 46.47 Å³, respectively. As Zn and Sn have larger ionic sizes than Ga, the unit cell was expected to become bigger after substitution of Ga with Zn and Sn. The full-width-half-maximum (FWHM) values of the (10 $\bar{1}$ 0) peak in terms of the 2θ value decreased from 0.54° for the 100°C-deposited film to 0.46° for the 400°C one. The smaller FWHM value indicates improved crystallinity at higher deposition temperature. The crystalline sizes were 15.3 nm, 16.2 nm, 17.2 nm, and 17.9 nm for films deposited 100°C, 200°C, 300°C, and 400°C, respectively. All the derived data from the XRD measurements were shown in Table II. The effect of RF sputter power on Zn/Sn-GaN is apparent.

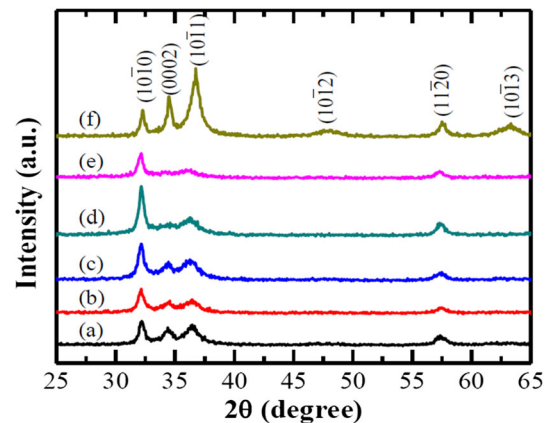


Fig. 1. XRD patterns of Zn acceptor/Sn donor codoped GaN films prepared at 120 W and different temperatures of (a) 100°C, (b) 200°C, (c) 300°C, and (d) 400°C, and at 400°C and different sputter powers of (e) 90 W, (d) 120 W, and (f) 150 W.

At the higher RF sputter power of 150 W, the diffraction peak from the (10 $\bar{1}$ 1) plane showed the highest intensity. The intensity magnitude of the diffraction peaks followed in the order: (10 $\bar{1}$ 1) > (0002) > (10 $\bar{1}$ 0) > (11 $\bar{2}$ 0) > (10 $\bar{1}$ 3). Diffraction peaks with multiple orientations were observed, indicating the randomized grain orientation. The FWHM value at (10 $\bar{1}$ 0) also showed the improved crystallinity for the 150 W-deposited film. The crystalline sizes were 17.6, 17.9, and 24.3 nm for films deposited 90 W, 120 W, and 150 W, respectively. At the lower RF sputter power of 90 W, the film showed the largest cell volume of 46.90 Å³. If the 90 W-deposited film with the $[N]/[metals] < 1$ is due to the nitrogen deficiency, the cell volume is expected to be smaller. If the lower nitrogen content is due to the metal interstitials, the cell volume of Zn/Sn-GaN can expand and be much larger. If the Zn/Sn excesses are to form grain boundary precipitates, the cell volume of 46.90 Å³ slightly expanding from 45.59 Å³ of pure GaN is due to the limited Zn/Sn solubility in GaN.

Figure 2 shows SEM surface morphologies of Zn acceptor/Sn donor codoped GaN films prepared at 120 W and different temperatures of (a) 100°C, (b) 200°C, (c) 300°C, and (d) 400°C, and at 400°C and different sputter powers of (e) 90 W, (d) 120 W, and

Table II. Structure properties of Zn/Sn-GaN thin films from the x-ray diffraction analyses

#	Sputter power (W)	Deposition temp. (°C)	2θ (10 $\bar{1}$ 0) peak	a (Å)	c (Å)	Volume (Å ³)	FWHM (10 $\bar{1}$ 0) (°)
(a)	120	100	32.20	3.20	5.20	46.38	0.54
(b)	120	200	32.15	3.21	5.20	46.47	0.51
(c)	120	300	32.15	3.21	5.20	46.47	0.48
(d)	120	400	32.15	3.21	5.21	46.62	0.46
(e)	90	400	32.05	3.22	5.21	46.90	0.53
(f)	150	400	32.30	3.19	5.19	46.01	0.34

(f) 150 W. For the effect of deposition temperature, all the Zn/Sn-GaN films were densely packed with small grains and the interface between the film and substrate was also dense without cracking. From the insets in each image, the films grown at 100°C, 200°C, 300°C, and 400°C were 0.87 μm , 0.88 μm , 0.92 μm , and 1.07 μm in thickness, respectively, or 29.3 nm/min, 29.5 nm/min, 30.8 nm/min, and 35.6 nm/min in growth rate. The film growth rate increased with the growth temperature. For the effect of RF power, Zn/Sn-GaN film showed the larger crystalline size at the higher RF sputter power. The film/substrate interface remained intact. The films grew faster at higher RF power. The films grown at 90 W, 120 W, and 150 W were 0.65 μm , 1.07 μm , and 1.33 μm in thickness, respectively, or 29.3 nm/min, 29.5 nm/min, and 35.6 nm/min in growth rate. From the cross-sectional images, no characteristic cracking traces were observed for the 100°C- and 200°C-deposited films with fine grains, but the traces from the cleavage planes became clear for films grown at higher growth temperatures at 300°C and 400°C with the larger grains, which were consistent with the XRD data. The cleavage traces became apparent for the 150 W-deposited films with the largest grains of 15–30 nm.

Figure 3 shows microstructural and structural characterizations of Zn acceptor/Sn donor codoped GaN films by microscopy. Figure 3a shows HR-TEM image of Zn/Sn-GaN film deposited at 120 W and 400°C with different lattice fringes from different grains. Lattice fringes of 2.77 Å from (10 $\bar{1}$ 0), 2.50 Å from (0002), and 2.43 Å from (10 $\bar{1}$ 1) were identified. It can be found that even the codoping of Zn and Sn does not lead to the formation of second phases at grain junctions. Twinning can be easily observed in Zn/Sn-GaN. The twinning behavior strongly corresponds to the internal stress due to the solid solution with cations of different charges and sizes. Figure 3b shows the selected area electron diffraction (SAED) pattern of Zn/Sn-GaN film. The major ring patterns from the (10 $\bar{1}$ 0), (10 $\bar{1}$ 1), (11 $\bar{2}$ 0), and (20 $\bar{2}$ 0) planes explain its single phase in polycrystalline nature. The intensity of ring pattern also indicates the relatively weak crystallization of Zn/Sn-GaN film. Figure 3c–f show the HAADF (high-angle annular dark-field imaging)-STEM-EDX

elemental maps of Ga, N, Zn, and Sn, respectively. It is observed from these maps that all the elements are evenly distributed over the sample.

The AFM topographies of Zn/Sn-GaN films after scanning at the $5 \times 5 \mu\text{m}^2$ area are showed in Fig. 4. The root-mean-square roughness values of Zn/Sn-GaN films decreased from 3.46 nm, 3.36 nm, 3.18 nm, to 2.90 nm, as the deposition temperatures increased from (a) 100°C, (b) 200°C, (c) 300°C, to (d) 400°C, respectively. The higher surface mobility for the adatoms from the sputter target due to the higher substrate temperature can make the atom packing on substrate improved and the film surface become smoother. For the RF power effect, the rms roughness values of 1.3 nm, 2.9 nm, and 4.2 nm were measured for films deposited at 90 W, 120 W, and 150 W, respectively. The high RF sputter power for film growth led to the rougher surface of Zn/Sn-GaN films. Basically, the surface roughness is the outcome between the competition of the sputter atom influx and the surface diffusion of adatoms with the faster growth rate at a higher RF power for the rougher surface. The RF power in this work had such high impact on the growth rate or on the sputter influx that high growth rate at high RF sputter power led to the rough surface. For films deposited at the fixed 120 W, their growth rates did not have a large difference at different substrate temperatures; therefore, the slightly higher growth rate had the smoother surface.

Electrical properties of Zn/Sn-GaN films prepared at different substrate temperatures and RF sputter powers were determined with the Hall measurement system at room temperature. For the effect of substrate temperature, the (a) carrier concentration, (b) mobility, and (c) electrical conductivity of Zn/Sn-GaN films are shown in Fig. 5. The Zn/Sn-GaN films made of the 6% Zn/4% Sn GaN target presented as a *p*-type semiconductor at different substrate temperatures. The carrier concentrations (n_p) were $1.2 \times 10^{15} \text{ cm}^{-3}$, $3.9 \times 10^{15} \text{ cm}^{-3}$, $9.9 \times 10^{15} \text{ cm}^{-3}$, and $1.8 \times 10^{16} \text{ cm}^{-3}$, mobilities (μ) were $42 \text{ cm}^2 \text{ V}^{-1} \text{ s}^{-1}$, $43 \text{ cm}^2 \text{ V}^{-1} \text{ s}^{-1}$, $34 \text{ cm}^2 \text{ V}^{-1} \text{ s}^{-1}$, and $23 \text{ cm}^2 \text{ V}^{-1} \text{ s}^{-1}$, and electrical conductivities (σ) were 0.008 S cm^{-1} , 0.03 S cm^{-1} , 0.05 S cm^{-1} , and 0.06 S cm^{-1} for Zn/Sn-GaN films prepared at 100°C, 200°C, 300°C, and 400°C,

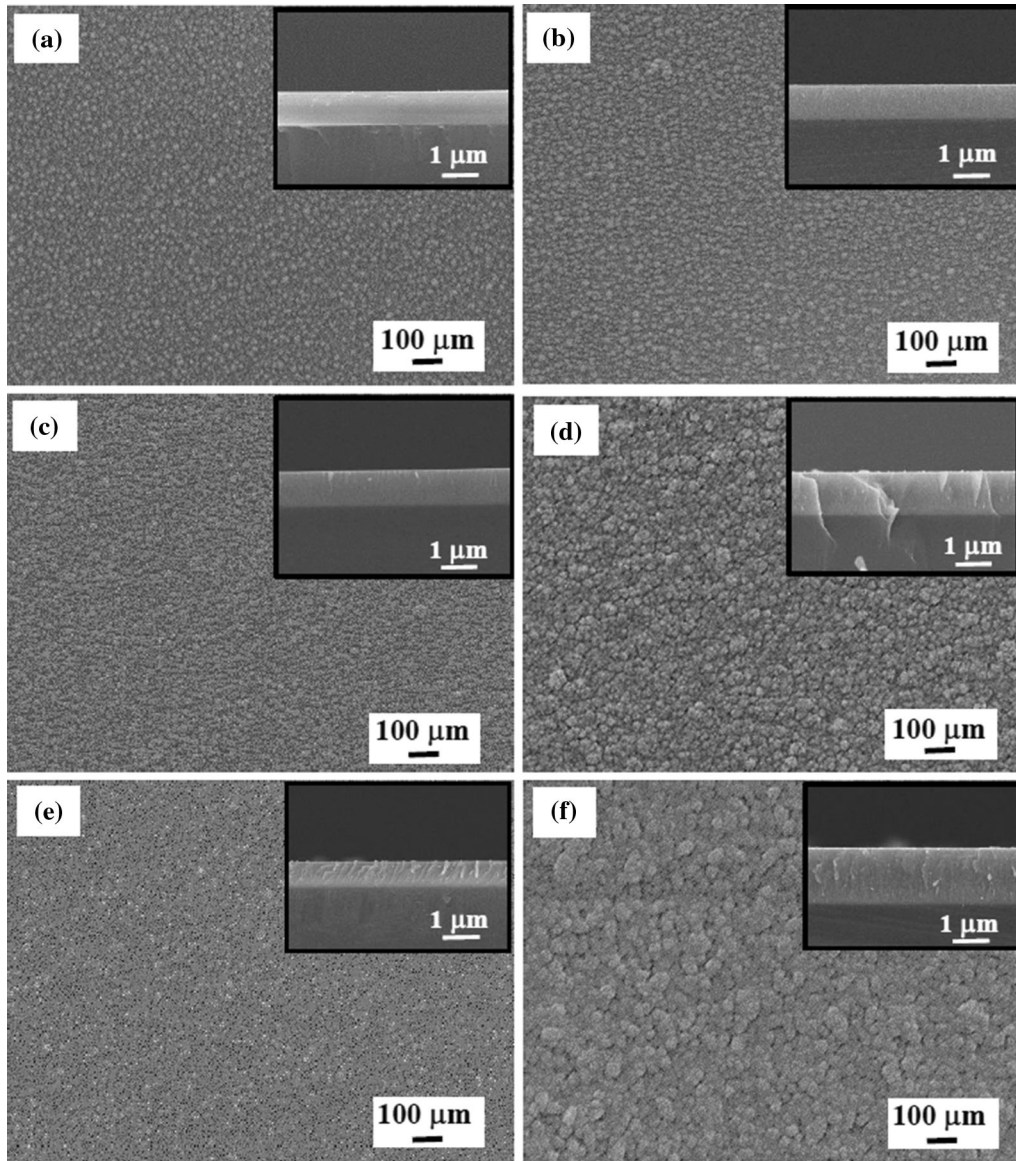


Fig. 2. SEM surface morphologies of Zn acceptor/Sn donor codoped GaN films prepared at 120 W and different temperatures of (a) 100°C, (b) 200°C, (c) 300°C, and (d) 400°C, and at 400°C and different sputter powers of (e) 90 W, (d) 120 W, and (f) 150 W. The insets their individual cross-sectional images.

respectively. The higher growth temperature improved the crystallinity for the enhanced hole concentration and the improved electrical conductivity due to the fewer defects. Pure GaN film grown at 400°C behaved as an *n*-type semiconductor with its carrier concentration of $1.47 \times 10^{16} \text{ cm}^{-3}$ and mobility of $118 \text{ cm}^2 \text{ V}^{-1} \text{ s}^{-1}$. For Sn-GaN film, it was an *n*-type semiconductor with the n_e value $> 10^{18} \text{ cm}^{-3}$, but much lower carrier mobility below $1 \text{ cm}^2 \text{ V}^{-1} \text{ s}^{-1}$.⁴ The Zn addition is actually working to adjust the electrical properties by the way of acceptor/donor codoping to simultaneously create the acceptor level and donor level in a controllable approach. Therefore, the high conductive Sn-doped GaN with high $n_e > 10^{18} \text{ cm}^{-3}$ can be changed to the low conductive *p*-type GaN of low $n_p \sim 10^{15}$

cm^{-3} with the addition of zinc acceptor, while maintained the high mobility of $30\text{--}40 \text{ cm}^2 \text{ V}^{-1} \text{ s}^{-1}$. Therefore, the Zn and Sn substitutions in GaN can improve the drawbacks of low mobility and high carrier concentration of Sn-GaN, but still provide the acceptor and donor functions for GaN. For the effect of RF sputter power, the (a) carrier concentration, (b) mobility, and (c) electrical conductivity of Zn/Sn-GaN films are shown in Fig. 6. The Zn/Sn-GaN films still behaved as a *p*-type semiconductor. The carrier concentrations (n_p) were $9.5 \times 10^{12} \text{ cm}^{-3}$, $1.8 \times 10^{16} \text{ cm}^{-3}$, and $5.1 \times 10^{17} \text{ cm}^{-3}$, mobilities (μ) were $31 \text{ cm}^2 \text{ V}^{-1} \text{ s}^{-1}$, $23 \text{ cm}^2 \text{ V}^{-1} \text{ s}^{-1}$, and $13 \text{ cm}^2 \text{ V}^{-1} \text{ s}^{-1}$, and electrical conductivities (σ) were $1.5 \times 10^{-6} \text{ S cm}^{-1}$, 0.06 S cm^{-1} , and 1.1 S cm^{-1} for Zn/Sn-GaN prepared at 90 W,

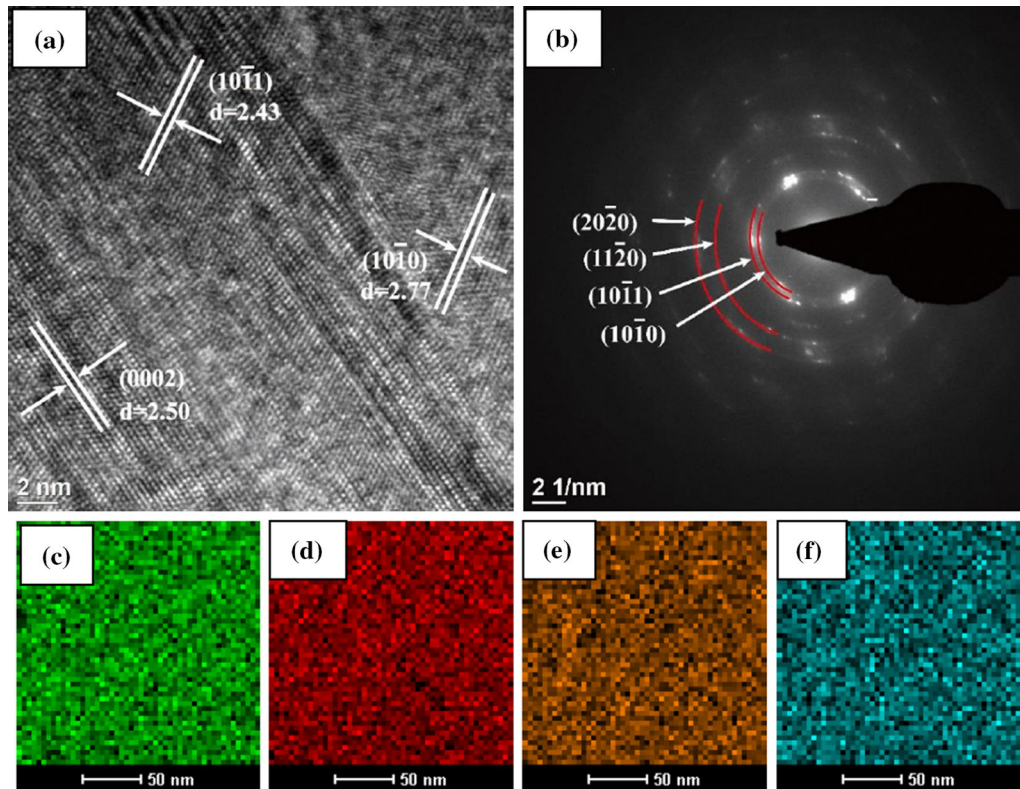


Fig. 3. Microstructural and structural characterizations of Zn acceptor/Sn donor codoped GaN films. (a) HR-TEM image, (b) SAED pattern, and EDX elemental mapping for (c) Ga, (d) N, (e) Zn, and (f) Sn.

120 W, and 150 W, respectively. The higher RF sputter power improved the crystallinity for the enhanced hole concentration and improved electrical conductivity. From the compositions listed in Table I, the variation of composition with RF power only showed the slightly lower Sn content for the 150 W-deposited film and the strongly deficient N content for the 90 W-deposited one, as the electrical properties largely changed with the RF sputter power (Fig. 6). From the extremely low n_p and σ values for the 90 W-deposited film, the Zn/Sn grain boundary precipitation can occur to block the charge transport path and to lower σ , while metal interstitials are also possible to provide the electrons from donor defect to compensate the hole concentration. On the other hand, the increased n_p and σ values of the p -type Zn/Sn-GaN prepared at 150 W can be related to the improved crystallinity and the lower Sn content at 3% instead of 4.8% or the lower donor concentration.

Optical band gap (E_g), an important optical property for semiconductors can be determined with UV-Vis spectrometer through the Tauc equation: $(\alpha h\nu)^2 = A(h\nu - E_g)$, where α is optical absorption coefficient, A a constant, and $h\nu$ the incident photon energy. The E_g values of the Zn/Sn-GaN films could be directly obtained by extrapolating each linear part of the $(\alpha h\nu)^2 - h\nu$ curves, as shown in Fig. 7. The extrapolated E_g values were 3.1 eV, 3.06 eV,

3.03 eV, and 3.0 eV for Zn/Sn-GaN films deposited at 100°C, 200°C, 300°C, and 400°C, while they were 3.22 eV, 3.0 eV, and 2.92 eV for films grown at 90 W, 120 W, and 150 W, respectively. The slightly changed E_g values for films deposited at different temperatures are consistent with the slightly changed compositions, as shown in Table I. Shikanai et al. studied $\text{Sn}_{0.4}\text{GaN}$ film and found the Sn_{Ga} donor level located 33 meV below conduction band.³ Zn-doped SnGaN films had found the Zn_{Ga} acceptor level located 200–400 meV above the valence band.^{24–26} Our band gap of 3.0 eV is contributed from the gap between the Zn_{Ga} acceptor and Sn_{Ga} donor levels. To explain the effect of RF sputter power on E_g , we need to consider from the composition difference: the slightly lower Sn content for the 150 W-deposited film and the strongly deficient N content for the 90 W-deposited one, as compared with the 120 W deposition condition. For the 150 W-deposited film, its 3% Sn content is much lower to compensate for the 7% Zn content. Therefore, more available Zn will be used for the Zn_{Ga} acceptor level and band gap becomes smaller to 2.92 eV due to the ΔE_g value being proportional to the carrier concentration for a degenerate semiconductor. Sanon et al. in 1990 proposed that band gap narrowing occurred, after films were heavily doped.²⁷ For the 90 W-deposited film with the higher E_g of 3.22 eV, we can derive that Zn/Sn grain boundary precipitation is

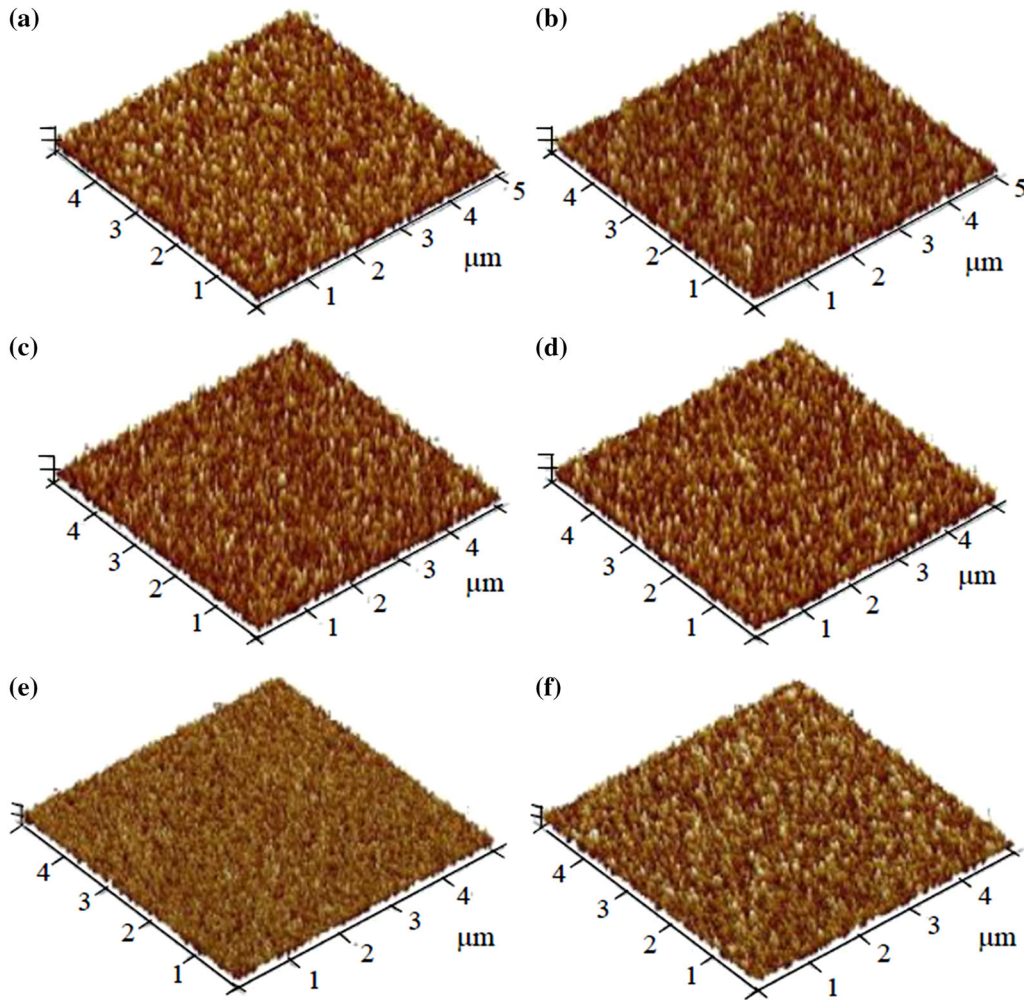


Fig. 4. 3D-AFM topographies of Zn acceptor/Sn donor codoped GaN films prepared at 120 W and different temperatures of (a) 100°C, (b) 200°C, (c) 300°C, and (d) 400°C, and at 400°C and different sputter powers of (e) 90 W, (d) 120 W, and (f) 150 W.

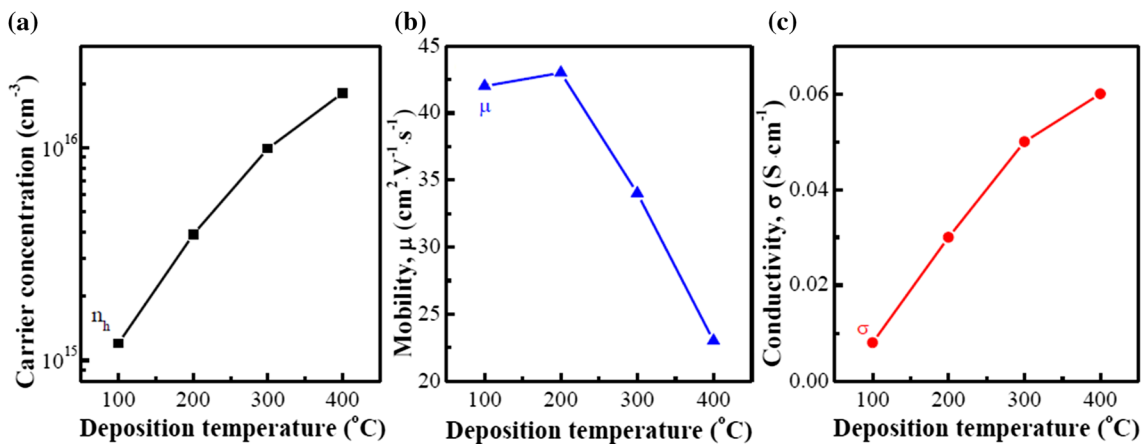


Fig. 5. Electrical properties of (a) carrier concentration, (b) mobility, and (c) electrical conductivity of Zn acceptor/Sn donor codoped GaN films prepared at 120 W and different temperatures.

the major contribution for the film defects. The fine precipitation around grain boundary does not interrupt the optical properties from the major phase of

grain, but can be a big problem for hole transport across the grain boundary. After precipitation, the grains have lower dopant concentration and the Zn/

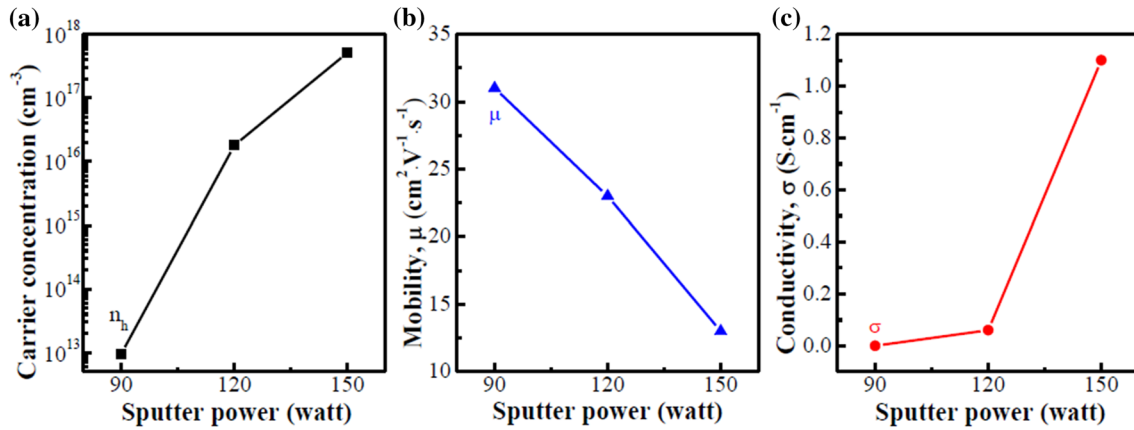


Fig. 6. Variations of electrical properties of (a) carrier concentration, (b) mobility, and (c) electrical conductivity of Zn acceptor/Sn donor codoped GaN films prepared at 400°C and different sputter powers.

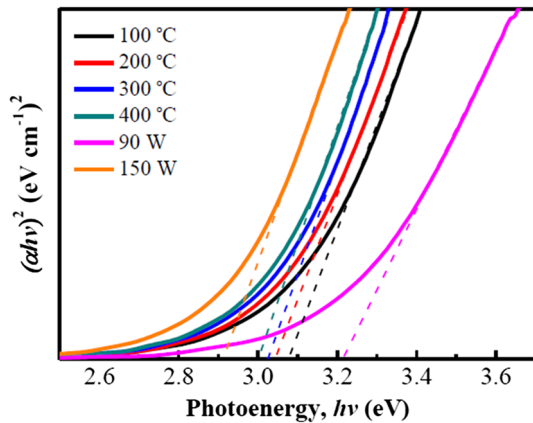


Fig. 7. Plots of $(\alpha hv)^2$ versus photon energy ($h\nu$) for the optical band gap measurements of Zn acceptor/Sn donor codoped GaN films prepared at 120 W and different temperatures of 100–400°C, and at 400°C and different sputter powers of 90–150 W.

Sn-GaN film can have higher E_g . If the film defect is made of metal interstitials, the donor and acceptor defect levels changed with the Zn and Sn contents will lead to a lower E_g value. The grain boundary precipitation of second phases indicates the RF sputter power needs to be higher than 90 W to improve the solid solubility of Zn and Sn. The band gap widening proposed as the Burstein–Moss effect²⁸ due to the higher donor defects and electron concentration is not observed on the 90 W-deposited film with extremely low n_p and low σ .

CONCLUSIONS

Acceptor/donor codoped Zn/Sn-GaN films have been successfully deposited on Si (100) substrates using reactive sputtering technique with a cermet target containing 6% Zn and 4% Sn. XRD, HR-TEM, SEM, AFM, and UV–Vis spectrometry were used to study the variations of microstructure and characteristics of Zn/Sn-GaN films with deposition

temperature and sputter power. All Zn/Sn-GaN films were in the polycrystalline form and formed a wurtzite structure. The RF sputter power had a strong effect on the performance of films. All Zn/Sn-GaN films were a p -type semiconductor. The hole concentrations were $9.5 \times 10^{12} \text{ cm}^{-3}$, $1.8 \times 10^{16} \text{ cm}^{-3}$, and $5.1 \times 10^{17} \text{ cm}^{-3}$, mobilities were $31 \text{ cm}^2 \text{ V}^{-1} \text{ s}^{-1}$, $23 \text{ cm}^2 \text{ V}^{-1} \text{ s}^{-1}$, and $13 \text{ cm}^2 \text{ V}^{-1} \text{ s}^{-1}$, and electrical conductivities were $1.5 \times 10^{-6} \text{ S cm}^{-1}$, 0.06 S cm^{-1} , and 1.1 S cm^{-1} for Zn/Sn-GaN prepared at 90 W, 120 W, and 150 W, respectively, while the optical band gap values were 3.22 eV, 3.0 eV, and 2.92 eV. Basically, the Zn/Sn codoping in GaN films needs to be grown above 90 W of the RF power to avoid the grain boundary precipitation from charge transport blocking. Through the processing control, our heavily acceptor/donor codoped, p -type GaN films with a variety of electrical properties can be achieved. This type of degenerated semiconductor with an easy process can have potentials in environmental and chemical sensing.

ACKNOWLEDGMENTS

This work was supported by the Ministry of Science and Technology of the Republic of China under Grant Nos. MOST 104-2221-E-011-169-MY3 and MOST 106-3111-Y-042A-093.

REFERENCES

1. S. Nakamura, T. Mukai, and M. Senoh, *Japan J. Appl. Phys.* 31, 2883 (1992).
2. S.I. Molina, A.M. Sánchez, F.J. Pacheco, R. García, M.A. Sánchez-García, F.J. Sánchez, and E. Calleja, *Appl. Phys. Lett.* 74, 3362 (1999).
3. A. Shikanaia, H. Fukahori, Y. Kawakami, K. Hazu, T. Sota, T. Mitani, T. Mukai, and S. Fujita, *Physica Status Solidi (b)* 235, 26 (2003).
4. C.W. Ting, C.P. Thao, and D.H. Kuo, *Mater. Sci. Semicond. Proc.* 59, 50 (2017).
5. S. Nakamura, T. Mukai, and M. Senoh, *Appl. Phys. Lett.* 64, 1687 (1994).
6. J.K. Sheu, C.J. Pan, G.C. Chi, C.H. Kuo, L.W. Wu, C.H. Chen, S.J. Chang, and Y.K. Su, *IEEE Photo. Technol. Lett.* 14, 450 (2002).

7. M.A. Reshchikov, M. Foussekis, J.D. McNamara, A. Behrends, A. Bakin, and A. Waag, *J. Appl. Phys.* 111, 073106 (2012).
8. K.S. Kim, G.M. Yang, and H.J. Lee, *Solid State Electron.* 43, 1807 (1999).
9. A.K. Singh, K.P. O'Donnell, P.R. Edwards, K. Lorenz, J.H. Leach, and M. Boćkowski, *J. Phys. D Appl. Phys.* 51, 065106 (2018).
10. C.P. Thao, D.-H. Kuo, and D.J. Jan, *Mater. Sci. Semicond. Proc.* 82, 126 (2018).
11. D.-H. Kuo and Y.-T. Liu, *J. Mater. Sci.* 53, 9099 (2018).
12. H. Katayama-Yoshida, R. Kato, and T. Yamamoto, *J. Cryst. Growth* 231, 428 (2001).
13. S.S. Kocha, M.W. Peterson, D.J. Arent, J.M. Redwing, M.A. Tischler, and J.A. Turner, *J. Electrochem. Soc.* 142, L238 (1995).
14. I.M. Huygens, K. Strubbe, and W.P. Gomes, *J. Electrochem. Soc.* 147, 1797 (2000).
15. K. Maeda, K. Teramura, N. Saito, Y. Inoue, H. Kobayashi, and K. Domen, *Pure Appl. Chem.* 78, 2267 (2006).
16. K. Maeda, K. Teramura, and K. Domen, *J. Catal.* 254, 198 (2008).
17. C.C. Li and D.-H. Kuo, *J. Mater. Sci.-Mater. Electron.* 25, 1404 (2014).
18. C.C. Li and D.-H. Kuo, *J. Mater. Sci.-Mater. Electron.* 25, 1942 (2014).
19. T.T.A. Tuan, D.-H. Kuo, C.C. Chen, and W.C. Yen, *J. Mater. Sci.-Mater. Electron.* 25, 3264 (2014).
20. D.-H. Kuo, T.T.A. Tran, C.C. Chen, and W.C. Yen, *Mater. Sci. Eng. B* 193, 13 (2015).
21. T.T.A. Tuan, D.-H. Kuo, A.D. Saragih, and G.-Z. Li, *Mater. Sci. Eng., B* 222, 18 (2017).
22. C.P. Thao and D.-H. Kuo, *Mater. Sci. Semicond. Proc.* 74, 336 (2018).
23. K. Lin and D.H. Kuo, *J Mater Sci-Mater Electron* 28, 43 (2017).
24. J. Neugebauer and C.G. Van de Walle, *J. Appl. Phys.* 85, 3003 (1999).
25. J.L. Lyons, A. Janotti, and C.G. Van de Walle, *J. Appl. Phys.* 52, 08JJ04 (2013).
26. D.O. Demchenko and M.A. Reshchikov, *Physical Review B* 88, 115204 (2013).
27. G. Sanon, R. Rup, and A. Mansingh, *Phys. Rev. B* 44, 5672 (1991).
28. I. Hamberg and C.G. Granqvist, *Phys. Rev. B* 30, 3240 (1984).